Title: S1PR3 mediates inflammatory pain and itch via distinct TRP channel-dependent pathways

Abbrev. Title: S1PR3 mediates inflammatory pain and itch

Authors and Affiliations: Rose Z. Hill[1], Takeshi Morita[1#], Rachel B. Brem[2, 3], Diana M. Bautista[1, 4*]

1. Department of Molecular and Cell Biology, University of California, Berkeley, CA 94720, USA.
2. Department of Plant and Microbial Biology, University of California, Berkeley, CA 94720, USA.
3. Buck Institute for Research on Aging, Novato, CA 94945, USA.
4. Helen Wills Neuroscience Institute, University of California, Berkeley, CA 94720, USA.

[#] Current Address: The Rockefeller University, New York, NY 10065, USA.

[*] Correspondence should be addressed to dbautista@berkeley.edu

Number of pages: 36

Number of figures: 7

Number of tables: 0

Number of words:

Abstract: 210
Introduction: 641
Discussion: 824

Conflict of interest: The authors declare no competing financial interests.

Acknowledgements: We would like to thank all members of the D.M.B laboratory for constructive feedback and criticism.

Abstract

In this work, we establish a role for the bioactive lipid sphingosine 1-phosphate (S1P) and its receptor S1PR3 in inflammatory thermal pain and itch. S1P injection elicited robust heat hypersensitivity, acute pain, and itch behaviors in mice, which were wholly dependent on S1PR3. S1P-evoked pain was entirely dependent on TRPV1 ion channels, whereas S1P-evoked itch was dependent on TRPA1. Consistent with our *in vivo* findings, we found that S1P activated subsets of both heat- and itch-sensitive dorsal root ganglion (DRG) neurons, and that activation was solely dependent on S1PR3, and not S1PR1. Our data support a model in which S1P elicits neuronal activation via two pathways in distinct subsets of somatosensory neurons. Gβγ-dependent activation of TRPA1 mediates S1PR3-evoked calcium responses in one subpopulation, whereas PLC-dependent activation of TRPV1 mediates S1PR3-evoked calcium responses in the other subpopulation. In the Complete Freund's Adjuvant (CFA) -induced inflammatory pain model, S1PR3-deficient mice failed to develop heat hypersensitivity, whereas mechanical hypersensitivity developed normally. Pharmacological blockade of S1PR3 activity or S1P production rapidly and selectively ameliorated heat hypersensitivity in wild-type mice treated with CFA. These data definitively identify S1PR3 as a mediator of thermal pain and itch, and, furthermore, demonstrate for the first time that elevated peripheral S1P is an essential driver of chronic inflammatory pain.

Significance Statement

Chronic pain is a major health problem with few effective treatments. Here, we show that the pro-inflammatory lipid, S1P, and its receptor S1PR3 are essential for thermal hypersensitivity and acute itch. Our results suggest that S1PR3 inhibitors or S1P modulators may be of interest as powerful and heretofore untested treatments for inflammatory pain and itch.

70 # Introduction

71 Hypersensitivity to thermal and mechanical stimuli is a hallmark of inflammatory pain. During
72 inflammation, immune cells, skin cells, and neurons release a slew of small molecules, lipids,
73 and proteins into the extracellular milieu collectively referred to as the “inflammatory soup” (Ji,
74 Xu, & Gao, 2014). A handful of these factors are known to directly modulate the activity of
75 peripheral sensory neurons, resulting in thermal and/or mechanical hypersensitivity (Chuang et
76 al., 2001; Tominaga, Wada, & Masu, 2001). While several transduction channels and sensory
77 neuronal populations mediating acute pain and itch have been identified (Basbaum, Bautista,
78 Scherrer, & Julius, 2009; Meixiong & Dong, 2017; Pinho-Ribeiro, Verri, & Chiu, 2017), the
79 molecular factors that drive thermal and mechanical hypersensitivity under inflammatory states
80 remains enigmatic (Ghasemlou, Chiu, Julien, & Woolf, 2015). For example, it is known that mice
81 lacking TRPV1 fail to develop thermal but not mechanical sensitization in a model of chronic
82 inflammatory pain (Caterina et al., 2000), yet the physiologically relevant molecular pathways
83 upstream of TRPV1 sensitization are not fully understood. And likewise, while the immune cells
84 that promote mechanical hypersensitivity in chronic inflammatory pain have been identified, the
85 signaling factors that promote that sensitization remain unclear (Ghasemlou et al., 2015).
86
87 Sphingosine 1-phosphate (S1P) is a bioactive sphingolipid associated with asthma, neuropathic
88 pain, inflammatory bowel disease, and psoriasis (Checa et al., 2015; Donoviel et al., 2015; Hou
89 & Fang, 2015; Myśliwiec et al., 2016; Patti et al., 2008; Rivera, Proia, & Olivera, 2008; F.
90 Roviezzo et al., 2015). S1P signaling via S1P Receptor 1 (S1PR1) facilitates the migration,
91 recruitment, and activation of immune cells (Cyster & Schwab, 2012; Matloubian et al., 2004).
92 Intriguingly, expression of both S1PR1 and S1PR3 has been reported in the somatosensory
93 ganglia (Camprubi-Robles et al., 2013; Usoskin et al., 2015), and S1P modulates sensory

94 neuronal excitability (Li, Li, Kays, Guerrero, & Nicol, 2015; Wang et al., 2017). However, the role
95 of S1P signaling in somatosensation remain unclear.
96
97 In this study, we elucidate the molecular mechanisms of S1P signaling in pain and itch. While
98 the subject of a number of previous studies, whether and how S1P signaling directly mediates
99 acute and inflammatory pain remains enigmatic for several reasons (Camprubi-Robles et al.,
100 2013; Canlas et al., 2015; Finley et al., 2013; Janes et al., 2014; Mair et al., 2011; Weth et al.,
101 2015). First, and foremost, the S1P receptors in sensory ganglia involved in S1P-evoked heat
102 hyperalgesia (Mair et al., 2011) and spontaneous pain behaviors (Camprubi-Robles et al., 2013)
103 have remained controversial. While both S1PR1 and S1PR3 have been implicated in
104 nociception, the aforementioned studies showed incomplete loss of S1P-evoked behaviors or
105 partial phenotypes. Localization studies were performed with anti- S1P receptor antibodies that
106 stain S1PR3-deficient sensory ganglia. As such, the sensory neuronal subtype(s) that
107 participate in S1P signaling are unknown. Additionally, these studies were cursory and did not
108 probe the downstream signaling pathways activated by S1P receptor(s) in sensory neurons.
109 These studies also employed excessively high concentrations of S1P in behavioral experiments,
110 two to three orders of magnitude higher than levels reported in mammals (0.1 nM – 10 μM), and
111 beyond the solubility limits of this lipid in saline (micromolar). Finally, no study has examined the
112 role of S1P signaling in itch sensation.
113
114 Here, we aimed to perform a rigorous and systematic characterization of the behavioral effects
115 and underlying mechanisms of S1P signaling in acute pain and itch and chronic inflammatory
116 pain. We have found that elevated S1P triggers acute pain, heat hypersensitivity, and,
117 surprisingly, itch behaviors that are wholly dependent on S1PR3. Intriguingly, S1PR3-deficient
118 mice do not develop thermal hypersensitivity in the CFA model of inflammatory pain. In addition,
119 acute pharmacological blockade of peripheral S1PR3 signaling or S1P production reverses

120 CFA-evoked thermal hypersensitivity. Our findings define new roles for S1PR3 signaling in pain
121 and itch and show that S1P itself is an essential contributor to inflammatory pain in the
122 periphery.
123

124 Materials and Methods

125 *Behavioral studies & mice*

126 *S1P$_3^{mcherry/+}$* (Sanna et al., 2015) and *S1pr3* $^{-/-}$ (Kono et al., 2004) mice were obtained from
127 Jackson Laboratory and backcrossed to C57bl6/J, *Trpv1*$^{-/-}$ and *Trpa1*$^{-/-}$ mice were described
128 previously (Bautista et al., 2006; Caterina et al., 2000) and *Trpv1*$^{-/-}$/*Trpa1*$^{-/-}$ mice were bred from
129 crossing *Trpv1*$^{-/+}$ and *Trpa1*$^{-/+}$ mice. Wherever possible, wild-type (for *Trpa1* and *Trpv1* behavior)
130 or wild-type/heterozygous (*S1pr3)* littermate controls were used in behavioral experiments. Mice
131 (20–30 g) were housed in 12 h light-dark cycle at 21°C. Mice were singly housed one week prior
132 to all behavioral experiments and were between 8-10 weeks at the time of the experiment. All
133 mice were acclimated in behavioral chambers on the 2 subsequent days for at least 1 hour prior
134 to treatment for itch/pain behavior and radiant heat. Male mice were used for all behavioral
135 studies, due to the effects of the female estrus cycle on itch and pain behaviors.
136

137 Itch and acute pain behavioral measurements were performed as previously described (Wilson
138 et al., 2011). Mice were shaved one week prior to itch behavior. Compounds injected: 200 nM, 2
139 μM, 10 μM S1P (Tocris, Avanti Polar Lipids), 500 μM TY 52156 (Tocris), and 50 μM SKI II
140 (Tocris) in PBS with either DMSO- or Methanol-PBS vehicle controls. Pruritogens were injected
141 using both the neck/rostral back model (20 μl), and the cheek model (20 μl) of itch, as
142 previously described (Wilson et al., 2011). Behavioral scoring was performed while blind to
143 experimental condition and mouse genotype. All scratching and wiping behavior videos were
144 recorded for 1 hour and scored for either the first 30 minutes (scratching) or the first five minutes

145 (wiping). Bout number, time spent scratching, and bout length were recorded for scratching
146 behavior. Wiping was recorded as number of wipes.
147
148 For radiant heat hypersensitivity behavior, S1P was injected intradermally into the plantar
149 surface of the hindpaw (20 µl). Radiant heat paw withdrawal latencies, before and after
150 application of compound or vehicle were performed as previously described (Morita et al., 2015;
151 Tsunozaki et al., 2013). Radiant heat assays were performed using the Hargreaves test system
152 (IITC Life Science). Mice were injected with compound of interest into the hind paw, and their
153 paw withdrawal latencies were measured 15 min pre- and 20 min-30 min post-injection. Valid
154 responses for radiant heat included fast paw withdrawal, licking/biting/shaking of the affected
155 paw, or flinching. Mice were allowed to acclimate on platform for 1 hour before injection.
156
157 For the CFA model of chronic inflammatory pain, 15 µl of CFA (Sigma-Aldrich) or PBS control
158 was injected into either the left or right hindpaw of 8-9 week old mice briefly anesthetized with
159 2% isoflurane. Experimenter was blind to genotype. Von Frey paw withdrawal latencies were
160 recorded as previously described (Tsunozaki et al., 2013) using the up-down method (Chaplan,
161 SR, Bach, FW, Pogrel, JW, Chung, JM, Yaksh, 1994; Dixon, 1980) on a mesh grate (IITC Life
162 Science) with calibrated filaments (Touch Test). Radiant heat withdrawal latencies were
163 measured at baseline, 24-, and 48-hours post-injection for both paws. Paw swelling was
164 measured using calipers while experimenter was blind to genotype. Photographs were taken
165 after mice were euthanized using CO_2 while photographer was blinded to genotype.
166
167 All behavior experiments were carried out using age-matched or littermate cohorts of male mice.
168 Mice were tested in 4-part behavior chambers (IITC Life Science) with opaque dividers (Tap
169 Plastics). Itch and acute pain behavior was filmed from below using high-definition cameras. All
170 experiments were performed under the policies and recommendations of the International

171 Association for the Study of Pain and approved by the University of California, Berkeley Animal
172 Care and Use Committee.
173
174 *Analysis of gene expression vs. itch correlation data*
175 A previous study examined the correlation of transcript expression of individual genes in dorsal
176 root ganglion (DRG) neurons with itch behavior among BXD mouse strains (Morita et al., 2015).
177 One of the top correlated genes from the screen was *Fam57b* (r = 0.57), a recently identified
178 ceramide synthase (Yamashita-Sugahara et al., 2013) and component of the S1P pathway that
179 is robustly expressed in somatosensory neurons (Gerhold et al., 2013). To assess whether
180 expression of the S1P pathway genes as a group was correlated with somatosensory behaviors
181 across the mouse strains of the BXD population, we first tabulated the absolute value of the
182 Pearson's correlation r between expression of each S1P pathway gene in turn (*Fam57b,*
183 *Ppargc1a, Spns1, Spns2, Sphk2, S1pr3, S1pr1, Esrrb, Esrrg, Lrp2*) and itch behavior (Morita et
184 al., 2015), and calculated the median of these correlation values, r_{true}. We then drew 10 random
185 genes from the set of all 16,220 genes with detected expression and computed the median
186 correlation as above using this null set, r_{null}. Repeating the latter 10,000 times established a null
187 distribution of median correlations; we took the proportion of resampled gene groups that
188 exhibited ($r_{true} \geq r_{null}$) as an empirical p-value reporting the significance of enriched correlation
189 between expression and itch in the genes of the S1P pathway.
190
191 *In situ hybridization (ISH)*
192 Fresh DRG were dissected from 8-12 week old mice, flash frozen in OCT embedding medium,
193 and sectioned at 14 μm onto slides. ISH was performed using Affymetrix Quantigene ViewISH
194 Tissue 2-plex kit according to manufacturer's instructions with Type 1 and Type 6 probes. The
195 following probes against mouse mRNAs were created by Affymetrix and used for ISH: *S1pr3,*
196 *Mrgpra3, Trpv1,* and *Trpa1.* Slides were mounted in Fluoromount with No. 1.5 coverglass.

197 Imaging of ISH experiments and all other live- and fixed-cell imaging was performed on an
198 Olympus IX71 microscope with a Lambda LS-xl light source (Sutter Instruments). Images were
199 analyzed using ImageJ software. Briefly, DAPI-positive cells were circled and their fluorescence
200 intensity (AFU) for all channels was plotted against cell size using IgorPro software. Co-labeling
201 analysis was performed using ImageJ. Intensity thresholds were set based on the negative
202 control staining slide. Cells were defined as “co-expressors” if their maximum intensities were
203 greater than the threshold for both the Type 1 and Type 6 probe channels.
204
205 *Cell culture*
206 Cell culture was carried out as previously described (Wilson et al., 2011). Briefly, neurons from
207 dorsal root ganglia of 2-8 week old male and female mice, or trigeminal ganglia from P0-P4
208 neonates were dissected and incubated for 10 min in 1.4 mg ml−1 Collagenase P (Roche) in
209 Hanks calcium-free balanced salt solution, followed by incubation in 0.25% standard trypsin
210 (vol/vol) -EDTA solution for 2 min with gentle agitation. Cells were then triturated, plated onto
211 Poly D-Lysine coated glass coverslips and used within 20 h. (media: MEM Eagle's with Earle's
212 BSS medium, supplemented with 10% horse serum (vol/vol), MEM vitamins,
213 penicillin/streptomycin and L-glutamine).
214
215 *Electrophysiology*
216 Current clamp experiments were carried out as previously described (Wilson et al., 2011).
217 Briefly, gap-free current-clamp recordings were collected at 5 kHz and filtered at 2 kHz
218 (Axopatch 200B, pClamp software). Electrode resistance ranged between 1.5–5 MΩ. Internal
219 solution contained 140 mM KCl, 5 mM EGTA and 10 mM HEPES (pH 7.4). Bath solution was
220 physiological Ringer’s solution. The pipette potential was canceled before seal formation.
221 Experiments were carried out only on cells with a series resistance of less than 30 MΩ. Analysis
222 of electrophysiology data was performed in pClamp and IgorPro.

223

224 *Calcium imaging*

225 Ca^{2+} imaging experiments were carried out as previously described (Wilson et al., 2011). DRG
226 neurons from 2-8 week old male and female mice were used for all experiments. Where
227 indicated, TG neurons were from P0-P4 neonates. When experiments were performed on non-
228 wild-type mice, an age-matched wild-type control was also prepared and imaged the same day.
229 Cells were loaded for 60 min at room temperature with 10 μM Fura-2AM supplemented with
230 0.01% Pluronic F-127 (wt/vol, Life Technologies) in a physiological Ringer's solution containing
231 (in mM) 140 NaCl, 5 KCl, 10 HEPES, 2 CaCl2, 2 MgCl2 and 10 D-(+)-glucose, pH 7.4. All
232 chemicals were purchased from Sigma. Acquired images were displayed as the ratio of 340 nm/
233 380 nm. Cells were identified as neurons by eliciting depolarization with high potassium Ringer's
234 solution (75 mM) at the end of each experiment. Responding neurons were defined as those
235 having a > 15% increase from baseline ratio. Image analysis and statistics were performed
236 using automated routines in Igor Pro (WaveMetrics). Fura-2 ratios were normalized to the
237 baseline ratio F340/F380 = (Ratio)/(Ratio t = 0).

238

239 *Flow cytometry of CFA-treated paws*

240 CFA injections were performed as described above. Briefly, hindpaw skin and underlying fascia
241 of treated and PBS-injected paws were removed from freshly euthanized mice. Skin was placed
242 in RPMI media (Gibco) on ice before mincing with dissection scissors. Digestions were
243 performed for 90 minutes at 37°C on a rotating platform in 1 mL RPMI supplemented with
244 1:1000 DNaseI enzyme (Roche) and 1 unit LiberaseTM (Roche). Skin was then filtered through
245 70 μm nylon mesh (Falcon), washed in RPMI, and resuspended in PBS for Aqua Live-Dead
246 staining. Samples were then transferred to FACS buffer (PBS with 0.5% FBS and 2 mM EDTA),
247 blocked, then surface stained with the following antibodies: cKit-Biotin, FceRI-PE, CD49b-
248 PECy7, SiglecF-APC, SA-FITC, Ly6C-PerCP, CD11b-PB, Ly6G-780, CD45.2-AF700.

249 Compensation tubes (single-stain) were prepared for each fluorophore using positive and
250 negative control beads. A spleen from a wild-type animal was also prepared by crushing
251 between frosted glass slides, straining through 70 µm nylon mesh, and lysing of erythrocytes in
252 ACK (Gibco). A portion of spleen sample was heat-killed for 10 minutes at 65°C and stained
253 with Aqua viability stain and set aside. The rest of the spleen was stained normally with the
254 other skin samples. Samples were then run through a flow cytometer (BD Fortessa). Data were
255 analyzed using FlowJo (Prism) and Microsoft Excel. Neutrophils were defined as live single cells
256 with the following staining profile: $CD45.2^{+}/CD11b^{+}/Ly6G^{+}/Ly6C^{+}$. Inflammatory monocytes were
257 defined as the following: $CD45.2^{+}/CD11b^{+}/Ly6G^{-}/Ly6C^{high}$. Total number of immune cells was
258 reported since neither genotype differed significantly between total number of live cells or total
259 number of CD45.2+ immune cells.
260
261 *Experimental design & statistical analyses*
262 All statistical analyses were performed using IgorPro software or Prism. Values are reported as
263 the mean ± SEM where multiple experiments are reported, and mean ± SD where one
264 experiment was performed with multiple wells (for calcium imaging) or mice (for behavior). For
265 comparison between two groups, Student's unpaired 2-tailed t-test was used. For single-point
266 comparison between > 2 groups, a one-way ANOVA followed by the Sidak's, Dunnett's or
267 Tukey's post hoc tests (where appropriate) were employed. For the time course comparison
268 between 2 groups, 2-way ANOVA was used and single comparison p-values were derived using
269 Sidak's multiple comparisons. For comparing distributions, a type 2 Kolmogorov-Smirnov test
270 was used. Number of mice or samples required to attain significance was not calculated
271 beforehand and was based on numbers used in similar behavioral studies. Significance was
272 labeled as: n.s., not significant, $p \geq 0.05$; *$p < 0.05$; **$p < 0.01$; ***$p < 0.001$.
273
274

275 # Results

276 Our group previously harnessed natural variation in somatosensory behaviors among
277 genetically distinct mouse strains to identify candidate transducers in DRG neurons (Morita et
278 al., 2015). Analysis of this dataset revealed the sphingosine 1-phosphate (S1P) signaling
279 pathway (Fig. 1a) had transcript expression that was significantly correlated with increased itch
280 behaviors (see Methods; $p = 0.0116$; Fig. 1b). We focused our study on S1PR3 because it was
281 the most highly expressed S1P receptor in the dorsal root ganglia (DRG) (Morita et al., 2015;
282 Usoskin et al., 2015).
283
284 **S1PR3 is the sole mediator of acute S1P-evoked pain and itch**
285 A handful of previous studies have suggested that S1P may promote acute pain and/or thermal
286 sensitization via various S1PRs in sensory neurons, neutrophils, and/or platelets (Camprubi-
287 Robles et al., 2013; Finley et al., 2013; Mair et al., 2011; Weth et al., 2015). Here, we sought to
288 address the specific contribution of S1PR3 signaling to S1P-evoked somatosensory behaviors
289 using physiologically relevant concentrations of S1P (Checa et al., 2015; Myśliwiec et al., 2016;
290 Sanna et al., 2004).
291
292 We first used the cheek assay, which allows for simultaneous discrimination of pain-evoked
293 wiping and itch-evoked scratching (Shimada & LaMotte, 2008). We observed that S1P injection
294 resulted in wiping behaviors in response to S1P concentrations at or above 2 μM in the first five
295 minutes after injection (Fig. 2a). We also found that S1P elicited robust scratching behaviors
296 (Fig. 2b) that developed with an average latency of 4 minutes 29 seconds ± 1 minute 37
297 seconds and persisted for at least 30 minutes. Scratching was elicited in response to a wider
298 range of S1P concentrations than wiping (0.2-10 μM versus 2-10 μM). Furthermore, we did not
299 observe scratching behaviors in response to the lowest tested dose, 50 nM S1P (data not
300 shown). For all subsequent S1P scratching behavioral assays where wiping was not quantified,

301 we injected 0.2 μM S1P into the rostral back and observed an average scratching time of 55.5 ±
302 7.6 seconds (N = 29 animals), which was significantly greater than scratching evoked by vehicle
303 (0.1% methanol-PBS; 11.1 ± 3.3 seconds, N = 23 animals). Our results from the cheek and
304 rostral back models are consistent with a role for S1P in promoting both acute pain and itch.
305 Consistent with a previous study (Finley et al., 2013), we observed robust heat hypersensitivity
306 after injection of S1P (Fig. 2c). However, the concentration at which we observed
307 hypersensitivity, 10 μM, is at least 20-fold lower than sensitizing or pain-inducing concentrations
308 previously reported in the literature (Camprubi-Robles et al., 2013; Finley et al., 2013; Mair et
309 al., 2011). Mechanical hypersensitivity was not observed (data not shown).
310
311 We next tested the requirement of S1PR3 to S1P-evoked itch and pain behaviors. *S1pr3* $^{-/-}$ mice
312 displayed significantly attenuated S1P-evoked scratching indistinguishable from vehicle injection
313 (10.6 ± 12.3 s versus 6.3 ± 6.2 s, respectively; Fig. 2e). *S1pr3*$^{-/-}$ mice additionally lacked the
314 robust heat hypersensitivity and cheek wiping in response to injection of 10 μM S1P we
315 observed in both *S1pr3*$^{+/+}$ and *S1pr3*$^{+/-}$ littermates (Fig 2d,f). As previously reported, we
316 observed no defects in baseline thermal sensitivity in *S1pr3*$^{-/-}$ mice. The complete loss of S1P-
317 evoked behaviors in S1PR3-deficient mice suggests that S1PR3 is the sole receptor by which
318 S1P signals in somatosensory neurons to drive heat hypersensitivity, pain, and itch.
319
320 **S1PR3 is expressed and functional in subsets of TRPV1+ thermal nociceptors and**
321 **TRPA1+ pruriceptors**
322 Our acute behavioral data suggest that S1P-evoked behaviors are mediated by activation of
323 thermal nociceptors and pruriceptors. We demonstrated by *in situ* hybridization (ISH) that 43%
324 of dorsal root ganglion cells express *S1pr3.* These neurons comprise two main populations:
325 medium-to-large diameter mechanonociceptors as well as small-diameter neurons. Here, in
326 order to address the role of S1PR3 in thermal pain and itch, we characterized the small-

327 diameter *S1pr3*+ neurons by performing co-ISH of *S1pr3* with known markers of C-nociceptor
328 populations. We found that 51% of *S1pr3*+ cells express *Trpv1*, 34.3% express *Trpa1*, and
329 11.6% express *Mrgpra3* (Fig. 3a). These were indeed small-diameter nociceptors and/or
330 pruriceptors (mean diameter of *Trpv1+/S1pr3*+ cells = 23.4 ± 8.2 μm). In summary, our cellular
331 localization data reveal two main populations of small-diameter *S1pr3*+ neurons: 1) *Trpv1*-
332 positive thermal nociceptors and, 2) *Trpa1*-positive cells, including *Mrgpra3*+ pruriceptors.
333 These results are consistent with our behavioral studies showing a role for S1PR3 in acute pain
334 and itch.
335
336 We next employed whole cell current-clamp measurements to test whether S1P was sufficient
337 for action potential firing. Indeed, 1 μM S1P evoked action potential firing in capsaicin-sensitive
338 neurons (Fig. 3b). As an independent strategy to complement our ISH and electrophysiology
339 studies, we employed an *S1pr3* mCherry reporter mouse, which produces functional S1PR3-
340 mCherry fusion protein. Using sensory neurons this mouse in ratiometric calcium imaging, we
341 found that 56.1 ± 22.4 % of mCherry-expressing neurons were activated by 1 μM S1P (Fig. 3c-d
342 and these cells had a mean diameter of 22.4 ± 1.0 μm. Furthermore, 51.1 ± 16.8% of capsaicin-
343 responsive neurons were mCherry+, indicating functional overlap with TRPV1+ thermal
344 nociceptors. This suggests that only small-diameter thermal nociceptors and/or pruriceptors are
345 activated by S1P.
346
347 Further characterization via calcium imaging in wild-type sensory neurons revealed that 1 μM
348 S1P activates 34.2% of neurons, which fall into two main populations: 22.6% are
349 TRPV1+/TRPA1+ neurons, which are capsaicin- and AITC-sensitive, and 11.6% are
350 TRPV1+/TRPA1- neurons, which are capsaicin-sensitive and AITC-insensitive (Fig. 3e). The
351 complete overlap of S1P-responsive neurons with TRPV1+ neurons suggests a role for S1P in
352 heat hypersensitivity. Previous studies have shown that the MrgprA3+ subpopulation of

353 TRPA1+ neurons are required for many forms of non-histaminergic acute and chronic itch (Han
354 et al., 2013; Wilson et al., 2011). In keeping with our hypothesized role for S1P in itch, 80% of
355 chloroquine-responsive MrgprA3+ neurons responded to S1P. Our findings are consistent with
356 a role for S1P in activation of thermal nociceptors that express TRPV1 and pruriceptors that
357 express TRPA1.
358
359 We thus sought to examine the contribution of S1PR3 to S1P-evoked neuronal activation, for
360 which the literature is contradictory and suggestive of contributions of both S1PRs 1 and 3.
361 Incubating cells with the S1PR3-selective antagonist TY 52156 significantly attenuated S1P-
362 evoked calcium transients (Fig. 3f). In contrast, the S1PR1-selective antagonist W146 had no
363 effect on S1P responses (Fig. 3f). Thus, we hypothesized that S1PR3 is required for S1P-
364 evoked calcium signals. In support of our hypothesis, cultured DRG and TG neurons isolated
365 from *S1pr3*$^{-/-}$ mice exhibited no calcium responses to 1 μM S1P, and displayed indistinguishable
366 AITC- and capsaicin-evoked responses compared to wild-type controls (Fig. 3g). These findings
367 show that S1PR3, but not S1PR1, is required for neuronal activation by S1P.
368
369 **S1P activates sensory neurons via distinct TRPV1- and TRPA1-dependent mechanisms.**
370 We set out to identify the molecular pathway underlying S1P-evoked calcium transients in
371 cultured mouse DRG sensory neurons. S1P responses were mediated solely by calcium influx,
372 as chelation of extracellular calcium with 10 mM EGTA abolished all responses (Fig. 4a),
373 suggesting that S1P triggers the opening of plasma membrane cation channels. We also
374 observed similar results with application of Ruthenium Red (Fig. 4b), a blocker of a number of
375 calcium-permeable ion channels, including TRP channels.
376
377 Since TRPA1 and TRPV1 have been shown to mediate GPCR-dependent calcium signaling
378 and activation in small-diameter sensory neurons, we asked whether either of these channels

379 mediated S1P-evoked neuronal activation. We found that the percentage of sensory neurons
380 exhibiting calcium transients in response to S1P application were reduced in neurons isolated
381 from both *Trpv1*$^{-/-}$ (24.4 ± 5.84% vs. 34.8 ± 6.25%) and *Trpa1* $^{-/-}$ mice (8.6 ± 4.3% vs. 34.8 ±
382 3.3%; Fig. 4c-d).
383
384 By ratiometric calcium imaging, we observed a dose-dependent increase in the percentage of
385 DRG neurons activated by S1P, with an EC_{50} of 104 nM and maximal activation at 1 μM (Fig.
386 4e). However, neurons which were responsive to both AITC and S1P exhibited a slightly lower
387 EC_{50} for S1P (102 nM), and were activated by lower S1P concentrations (10 nM) than neurons
388 which were responsive to capsaicin and S1P (EC_{50} : 155 nM). This supports the notion that
389 S1P-evoked neuronal activation via TRPV1 and TRPA1 may occur in different populations of
390 sensory neurons, rather than through A1/V1 crosstalk in the same cells.
391
392 We also performed ratiometric calcium imaging on wild-type DRG neurons treated with the
393 TRPV1 antagonist capsazepine (50 μM) or the TRPA1 antagonist HC-030031 (50 μM). HC-
394 030031 significantly reduced S1P responses by ~78% (HC: 3.673 ± 1.568% vs. Veh: 17 ±
395 2.19%) whereas capsazepine significantly attenuated S1P responses by only ~50% (8.69 ±
396 0.865% vs. 17 ± 2.19%; Fig. 4f). Neurons isolated from mice lacking both TRPA1 and TRPV1
397 showed S1P responses similar to those evoked by vehicle (Fig. 4g).
398
399 We asked whether activation of sensory neurons by S1P/S1PR3 could be due to different G-
400 protein coupled mechanisms in distinct neuronal subpopulations. We found that inhibition of
401 PLC signaling using the drug U73122 blocked 42.4% of S1P-evoked calcium responses,
402 whereas the Gβγ blocker gallein attenuated 73.2% of S1P responses (Fig. 4h). Further
403 experiments showed that gallein and U73122 attenuate calcium responses to S1P in AITC-
404 sensitive neurons (S1P + vehicle: 22% S1P+/AITC+; S1P + Gallein: 6.2% S1P+/AITC+; S1P +

405 U73122: 11.2% S1P+/AITC+) with gallein causing much greater attenuation, whereas U73122
406 attenuates the majority of responses in capsaicin-sensitive, AITC-insensitive neurons (S1P +
407 vehicle: 14.5% S1P+/CAP+; S1P + U73122: 1.6% S1P+/CAP+). Our results with the G-protein
408 inhibitors mirror our observed proportions of TRPA1+ and TRPA1- S1P-responsive neurons,
409 suggesting that S1PR3 may signal primarily via PLC to activate TRPV1 and via Gβγ and/or PLC
410 to activate TRPA1, similar to the behavior of other excitatory GPCRs that signal via these
411 channels in somatosensory neurons (Imamachi et al., 2009; Morita et al., 2015; Wilson et al.,
412 2011). Overall, our data suggest that S1PR3 signaling opens TRPA1 or TRPV1 channels in two
413 distinct subpopulations of DRG neurons via canonical G-protein coupled mechanisms.
414

415 **S1P elicits pain and itch via distinct molecular pathways**

416 We hypothesized that the heat-sensor TRPV1 would be required for S1P-evoked acute pain
417 and heat hypersensitivity; however, we could not predict whether S1P-evoked itch would be
418 transduced via the TRPV1-dependent or TRPA1-dependent itch pathways. To this end, we
419 tested the requirement of TRPA1 and TRPV1 to S1P-evoked itch and pain behaviors. In both
420 the cheek wiping and radiant heat assays, S1P injection elicited robust acute pain and heat
421 hypersensitivity behaviors in wild type and *Trpa1*$^{-/-}$ mice, but not in *Trpv1*$^{-/-}$ mice (Fig. 5a,c).
422 Wild-type and *Trpv1*$^{-/-}$, but not *Trpa1*$^{-/-}$ mice, exhibited robust scratching behaviors to S1P that
423 were significantly greater than vehicle (Fig. 5b). Thus we concluded that S1P-evoked
424 spontaneous pain behaviors and heat hypersensitivity are mediated by TRPV1 and that S1P-
425 evoked itch is mediated by TRPA1, a known transducer of acute and chronic itchy stimuli
426 (Wilson et al., 2011, 2013). Overall, our results highlight a key role for S1PR3 signaling through
427 distinct molecular pathways in S1P-evoked acute pain, heat hypersensitivity, and itch.
428

429 **S1P and S1PR3 are essential for chronic thermal hypersensitivity**

430 The Complete Freund's Adjuvant (CFA) model of chronic inflammatory hypersensitivity is widely
431 used as a model of peripheral inflammation, but the molecular basis of pain hypersensitivity in
432 this model is incompletely understood. Injection of CFA into the hindpaw causes significant
433 thermal and mechanical hypersensitivity and swelling in wild type animals. In this model,
434 thermal hypersensitivity is dependent on TRPV1 ion channels (Caterina et al., 2000), although
435 the upstream mechanisms of TRPV1 sensitization in CFA are unclear (Boyce et al., 1996).
436 Additionally, paw edema in this model is due to extensive plasma extravasation, in which
437 soluble components of blood plasma are exposed to the skin. S1P, which is present at
438 concentrations 10- to 100-fold higher in blood plasma than in peripheral tissue, presents itself as
439 an attractive but unstudied component of the CFA inflammatory soup.
440
441 We therefore explored the role of S1PR3 in the CFA model of inflammatory pain. A variety of
442 immune cells infiltrate into the hindpaw following CFA treatment, and a recent study has shown
443 that myeloid cells are the principal driver of CFA-evoked mechanical but not thermal
444 hypersensitivity (Ghasemlou et al., 2015). Because S1P plays a key role in immune cell
445 migration, we asked whether *S1pr3*$^{-/-}$ displayed normal CFA-evoked immune cell infiltration into
446 the hindpaw. We observed no difference between *S1pr3*$^{-/-}$ and $^{+/-}$ animals among all immune cell
447 subtypes quantified (Fig. 6a-b), in support of previous studies showing that S1PR1 is the
448 primary mediator of S1P signaling in immune cells.
449
450 We next compared CFA-evoked hypersensitivity between *S1pr3*$^{+/-}$ and *S1pr3*$^{-/-}$ littermates, as no
451 significant differences were observed between *S1pr3*$^{+/+}$ and *S1pr3*$^{+/-}$ animals (Fig. 6). Strikingly,
452 *S1pr3*$^{-/-}$ animals failed to develop heat hypersensitivity (Fig. 6c), and displayed mild attenuation
453 of hindpaw swelling (Fig. 6d), similar to what has been reported for CFA-treated TRPV1-
454 deficient animals (Caterina et al., 2000). We therefore hypothesized that S1P levels become
455 elevated under inflammatory conditions, and that this promotes heat hypersensitivity via S1PR3-

456 mediated sensitization of TRPV1. In support of our hypothesis, acute blockade of S1P
457 production with SKI II (Chiba, Takeuchi, Sakai, & Misawa, 2010) rapidly reversed CFA heat
458 hypersensitivity (Fig. 6e). Furthermore, acute S1PR3 blockade with TY elevated heat-evoked
459 withdrawal latencies to pre-CFA, baseline levels (Fig. 6e). These results demonstrate that
460 peripheral S1P promotes CFA-evoked heat hypersensitivity via S1PR3 signaling and is a
461 component of the inflammatory soup that actively signals to promote pain.
462

463 ## Discussion

464 S1P is a bioactive signaling lipid best known for its essential roles in immune cell migration,
465 maturation, and activation via S1PR1 (Matloubian et al., 2004; Roviezzo et al., 2011; Schwab et
466 al., 2005). Recent studies have linked aberrant S1P signaling to a variety of diseases, including:
467 asthma, multiple sclerosis, cancer, psoriasis, and pain (Brinkmann et al., 2010; Checa et al.,
468 2015; Liang et al., 2013; Myśliwiec et al., 2016; Patti et al., 2008; Rivera et al., 2008; F.
469 Roviezzo et al., 2015). Yet the cellular and molecular targets of S1P in these disorders are
470 largely unknown. Here, we show that S1PR3 is the sole mediator of S1P-evoked pain and itch
471 and that S1P signaling is essential to chronic heat hypersensitivity (Fig. 7a), highlighting the
472 potential for a direct contribution of S1P to sensitization, pain and/or itch in these diseases.
473

474 **S1P evokes pain and itch via S1PR3**

475 The role of S1P in acute pain and pain hypersensitivity has been controversial. There are
476 conflicting reports of whether S1P mediates acute flinching and licking pain behaviors, and/or
477 thermal and mechanical hypersensitivity (Camprubi-Robles et al., 2013; Finley et al., 2013; Mair
478 et al., 2011; Weth et al., 2015). Likewise, these previous studies employed high-micromolar or
479 millimolar concentrations of S1P in mouse behavioral experiments, leaving it unclear whether
480 physiologically relevant S1P levels could contribute to somatosensation. Here we have shown
481 that physiological levels of S1P (nanomolar to low micromolar) are sufficient to evoke

482 somatosensory behaviors. We demonstrate that S1P triggers acute pain and heat
483 hypersensitivity via the noxious heat-sensing ion channel TRPV1. Additionally, S1P promotes
484 itch-evoked scratching that is dependent on the irritant-sensing ion channel TRPA1. While a
485 number of previous studies have implicated both S1PR1 and 3 in somatosensory neuron
486 function (Camprubi-Robles et al., 2013; Mair et al., 2011), several lines of evidence
487 unequivocally show that S1PR3 is the sole mediator of S1P-evoked pain and itch. First, DRG
488 neurons isolated from S1PR3-deficient animals do not respond to S1P. Second, application of
489 an S1PR3-selective antagonist, but not an S1PR1-selective antagonist, attenuates S1P
490 responses in cultured DRG neurons. Finally, S1PR3-deficient mice display no S1P-evoked
491 scratching, wiping, or heat hypersensitivity.
492
493 We also show for the first time that S1P acts as a pruritogen to evoke acute itch. Recent studies
494 have shown that circulating S1P levels are increased in chronic itch patients (from ~0.1 to 2 μM
495 in healthy versus chronic itch patients; Checa et al., 2015; Myśliwiec et al., 2016). S1PR3-
496 deficient mice displayed a complete loss of S1P-evoked itch behaviors. Future studies will
497 explore the role of S1P/S1PR3 signaling in chronic itch models to ascertain the pathological
498 relevance of S1P-evoked itch.
499
500 **S1PR3 mediates inflammatory thermal pain**
501 In the CFA model of inflammatory pain, both mechanical and thermal hypersensitivity occur with
502 distinct time courses, suggesting differential modes of regulation (Ghasemlou et al., 2015). It is
503 well-established that TRPV1 is required for CFA-evoked thermal hypersensitivity (Caterina et
504 al., 2000). We now show that S1PR3 activation can lead to opening of TRPV1 channels, and
505 that both S1PR3 and elevated S1P are required for CFA-evoked thermal hypersensitivity. These
506 data suggest that S1P may be an important contributor to inflammatory pain. Consistent with
507 this hypothesis, S1PR3-deficient mice display partial attenuation of paw swelling, a hallmark of

508 neurogenic inflammation, but still develop mechanical hypersensitivity, which has been
509 previously been shown to depend on infiltration of myeloid cells which display normal infiltration
510 in the S1PR3 knockout animals. S1PR3 signaling in neurons may generally contribute to pain
511 under inflammatory conditions. Plasma extravasation and edema, common symptoms of
512 inflammation, may increase local S1P concentrations and contribute to sensitization. Moreover,
513 we use pharmacology to show that active S1P signaling is required to maintain chronic heat
514 hypersensitivity.
515
516 Our findings suggest sensory neuronal S1PR3 may play roles in a host of disorders linked to
517 S1P signaling. Although S1P is produced by nearly every cell type, blood plasma contains the
518 highest levels of S1P (low micromolar), and S1P is secreted in large amounts by activated mast
519 cells (Olivera, Allende, & Proia, 2013; F. Roviezzo et al., 2015). Others have shown that
520 sensory neurons innervating the lung express *S1pr3* and that administration of a non-selective
521 S1P receptor agonist can enhance asthma-like airway hyperreactivity after acetylcholine
522 challenge (Trankner, Hahne, Sugino, Hoon, & Zuker, 2014). It is also well known that TRPV1+
523 sensory afferents are required for airway hypersensitivity (Rogerio, Andrade, & Calixto, 2011).
524 Furthermore, mast cells, which release S1P when activated (Kalesnikoff & Galli, 2008), play
525 important roles in allergic asthma as well as itch, and we propose that S1PR3 may play an
526 important role in mediating itch and/or airway hyperreactivity under these conditions.
527
528 Several S1PR modulators are currently in clinical trial for diseases linked to pain and/or itch,
529 including multiple sclerosis, IBD, and psoriasis (Brinkmann et al., 2010; Degagné & Saba, 2014;
530 Kunkel, Maceyka, Milstien, & Spiegel, 2013). While these drugs are intended to target the
531 immune system, we propose neuronal S1P/S1PR3 signaling as a potential target for the
532 treatment of inflammatory pain and itch.
533

534 # References

535 Basbaum, A. I., Bautista, D. M., Scherrer, G., & Julius, D. (2009). Cellular and Molecular
536 Mechanisms of Pain. *Cell*, *139*(2), 267–284. http://doi.org/10.1016/j.cell.2009.09.028

537 Bautista, D. M., Jordt, S. E., Nikai, T., Tsuruda, P. R., Read, A. J., Poblete, J., … Julius, D.
538 (2006). TRPA1 Mediates the Inflammatory Actions of Environmental Irritants and
539 Proalgesic Agents. *Cell*, *124*(6), 1269–1282. http://doi.org/10.1016/j.cell.2006.02.023

540 Boyce, S., Rupniak, N. M., Carlson, E. J., Webb, J., Borkowski, J. A., Hess, J., … Hill, R. G.
541 (1996). Nociception and inflammatory hyperalgesia in B2 bradykinin receptor knockout
542 mice. *Immunopharmacology*, *33*, 333–335. http://doi.org/10.1007/s00467-008-0901-
543 3.Dopamine

544 Brinkmann, V., Billich, A., Baumruker, T., Heining, P., Schmouder, R., Francis, G., … Burtin, P.
545 (2010). Fingolimod (FTY720): discovery and development of an oral drug to treat multiple
546 sclerosis. *Nat Rev Drug Discov*, *9*(11), 883–897. http://doi.org/10.1038/nrd3248

547 Camprubi-Robles, M., Mair, N., Andratsch, M., Benetti, C., Beroukas, D., Rukwied, R., …
548 Camprubí-Robles, M. (2013). Sphingosine-1-phosphate-induced nociceptor excitation and
549 ongoing pain behavior in mice and humans is largely mediated by S1P3 receptor. *J*
550 *Neurosci*, *33*(6), 2582–2592. http://doi.org/10.1523/jneurosci.4479-12.2013

551 Canlas, J., Holt, P., Carroll, A., Rix, S., Ryan, P., Davies, L., … Haberberger, R. V. (2015).
552 Sphingosine kinase 2-deficiency mediated changes in spinal pain processing. *Frontiers in*
553 *Molecular Neuroscience*, *8*(August), 1–13. http://doi.org/10.3389/fnmol.2015.00029

554 Caterina, M. J., Leffler, A., Malmberg, A. B., Martin, W. J., Trafton, J., Petersen-Zeitz, K. R., …
555 Julius, D. (2000). Impaired Nociception and Pain Sensation in Mice Lacking the Capsaicin

556 Receptor. *Science*, *288*(5464), 306–313. http://doi.org/10.1126/science.288.5464.306

557 Chaplan, SR, Bach, FW, Pogrel, JW, Chung, JM, Yaksh, T. (1994). Quantitative assessment of
558 tactile allodynia evoked by unilateral ligation of the fifth and sixth lumbar nerves in the rat.
559 *Journal of Neuroscience*, *53*, 55–63.

560 Checa, A., Xu, N., Sar, D. G., Haeggström, J. Z., Ståhle, M., & Wheelock, C. E. (2015).
561 Circulating levels of sphingosine-1-phosphate are elevated in severe, but not mild psoriasis
562 and are unresponsive to anti-TNF-α treatment. *Scientific Reports*, *5*(July), 12017.
563 http://doi.org/10.1038/srep12017

564 Chiba, Y., Takeuchi, H., Sakai, H., & Misawa, M. (2010). SKI-II, an inhibitor of sphingosine
565 kinase, ameliorates antigen-induced bronchial smooth muscle hyperresponsiveness, but
566 not airway inflammation, in mice. *Journal of Pharmacological Sciences*, *114*, 304–310.
567 http://doi.org/10.1254/jphs.10202FP

568 Chuang, H. H., Prescott, E. D., Kong, H., Shields, S., Jordt, S. E., Basbaum, a I., … Julius, D.
569 (2001). Bradykinin and nerve growth factor release the capsaicin receptor from
570 PtdIns(4,5)P2-mediated inhibition. *Nature*, *411*(6840), 957–962.
571 http://doi.org/10.1038/35082088

572 Cyster, J. G., & Schwab, S. R. (2012). Sphingosine-1-Phosphate and Lymphocyte Egress from
573 Lymphoid Organs. *Annual Review of Immunology*, *30*(1), 69–94.
574 http://doi.org/10.1146/annurev-immunol-020711-075011

575 Degagné, E., & Saba, J. D. (2014). S1 pping fire: Sphingosine-1-phosphate signaling as an
576 emerging target in inflammatory bowel disease and colitis-associated cancer. *Clinical and*
577 *Experimental Gastroenterology*, *7*(1), 205–214. http://doi.org/10.2147/CEG.S43453

578 Dixon, W. J. (1980). The Up-and-Down Method for Small Samples. *Journal of the American*
579 *Statistical Association*, *60*(312), 967–978.

580 Donoviel, M. S., Hait, N. C., Ramachandran, S., Maceyka, M., Takabe, K., Milstien, S., …
581 Spiegel, S. (2015). Spinster 2, a sphingosine 1-phosphate transporter, plays a Critical Role
582 in inflammatory and Autoimmune Diseases. *The FASEB Journal : Official Publication of the*
583 *Federation of American Societies for Experimental Biology*, *29*(12), 5018–5028.
584 http://doi.org/10.1096/fj.15-274936

585 Finley, a, Chen, Z., Esposito, E., Cuzzocrea, S., Sabbadini, R., & Salvemini, D. (2013).
586 Sphingosine 1-phosphate mediates hyperalgesia via a neutrophil-dependent mechanism.
587 *PLoS One*, *8*(1), e55255. http://doi.org/10.1371/journal.pone.0055255

588 Gerhold, K. a., Pellegrino, M., Tsunozaki, M., Morita, T., Leitch, D. B., Tsuruda, P. R., …
589 Bautista, D. M. (2013). The Star-Nosed Mole Reveals Clues to the Molecular Basis of
590 Mammalian Touch. *PLoS ONE*, *8*(1). http://doi.org/10.1371/journal.pone.0055001

591 Ghasemlou, N., Chiu, I. M., Julien, J.-P., & Woolf, C. J. (2015). CD11b $^{+}$ Ly6G $^{-}$ myeloid cells
592 mediate mechanical inflammatory pain hypersensitivity. *Proceedings of the National*
593 *Academy of Sciences*, 201501372. http://doi.org/10.1073/pnas.1501372112

594 Han, L., Ma, C., Liu, Q., Weng, H., Cui, Y., Tang, Z., … Dong, X. (2013). A subpopulation of
595 nociceptors specifically linked to itch. *Nature Neuroscience*, *16*(2), 174–182.
596 http://doi.org/10.1038/nn.3289.A

597 Hou, J.-C., & Fang, X.-M. (2015). S1P-S1PRs Alliance in Neuropathic Pain Processing. *Journal*
598 *of Anaesthesia and Perioperative Medicine*, *2*, 1–9.

599 Imamachi, N., Park, G. H., Lee, H., Anderson, D. J., Simon, M. I., Basbaum, A. I., & Han, S.-K.

600 (2009). TRPV1-expressing primary afferents generate behavioral responses to pruritogens
601 via multiple mechanisms. *Proceedings of the National Academy of Sciences of the United*
602 *States of America*, *106*(27), 11330–11335. http://doi.org/10.1073/pnas.0905605106

603 Janes, K., Little, J. W., Li, C., Bryant, L., Chen, C., Chen, Z., … Salvemini, D. (2014). The
604 development and maintenance of paclitaxel-induced neuropathic pain require activation of
605 the sphingosine 1-phosphate receptor subtype 1. *Journal of Biological Chemistry*, *289*(30),
606 21082–21097. http://doi.org/10.1074/jbc.M114.569574

607 Ji, R.-R., Xu, Z.-Z., & Gao, Y.-J. (2014). Emerging targets in neuroinflammation-driven chronic
608 pain. *Nature Reviews. Drug Discovery*, *13*(7), 533–48. http://doi.org/10.1038/nrd4334

609 Kalesnikoff, J., & Galli, S. J. (2008). New developments in mast cell biology. *Nature*
610 *Immunology*, *9*(11), 1215–23. http://doi.org/10.1038/ni.f.216

611 Kono, M., Mi, Y., Liu, Y., Sasaki, T., Allende, M. L., Wu, Y. P., … Proia, R. L. (2004). The
612 sphingosine-1-phosphate receptors S1P1, S1P2, and S1P3 function coordinately during
613 embryonic angiogenesis. *Journal of Biological Chemistry*, *279*(28), 29367–29373.
614 http://doi.org/10.1074/jbc.M403937200

615 Kunkel, G. T., Maceyka, M., Milstien, S., & Spiegel, S. (2013). Targeting the sphingosine-1-
616 phosphate axis in cancer, inflammation and beyond. *Nature Reviews. Drug Discovery*,
617 *12*(9), 688–702. http://doi.org/10.1038/nrd4099

618 Li, C., Li, J., Kays, J., Guerrero, M., & Nicol, G. D. (2015). Sphingosine 1-phosphate enhances
619 the excitability of rat sensory neurons through activation of sphingosine 1-phosphate
620 receptors 1 and/or 3. *Journal of Neuroinflammation*, *12*(1), 1–20.
621 http://doi.org/10.1186/s12974-015-0286-8

Liang, J., Nagahashi, M., Kim, E. Y., Harikumar, K. B., Yamada, A., Huang, W. C., … Spiegel, S. (2013). Sphingosine-1-Phosphate Links Persistent STAT3 Activation, Chronic Intestinal Inflammation, and Development of Colitis-Associated Cancer. *Cancer Cell*, *23*(1), 107–120. http://doi.org/10.1016/j.ccr.2012.11.013

Mair, N., Benetti, C., Andratsch, M., Leitner, M. G., Constantin, C. E., Camprubí-Robles, M., … Haberberger, R. V. (2011). Genetic evidence for involvement of neuronally expressed s1P1 receptor in nociceptor sensitization and inflammatory pain. *PLoS ONE*, *6*(2). http://doi.org/10.1371/journal.pone.0017268

Matloubian, M., Lo, C. G., Cinamon, G., Lesneski, M. J., Xu, Y., Brinkmann, V., … Cyster, J. G. (2004). Lymphocyte egress from thymus and peripheral lymphoid organs is dependent on S1P receptor 1. *Nature*, *427*(6972), 355–360. http://doi.org/10.1038/nature02284

Meixiong, J., & Dong, X. (2017). Annual Review of Genetics Mas-Related G Protein – Coupled Receptors and the Biology of Itch Sensation. http://doi.org/10.1146/annurev-genet-120116-024723

Morita, T., McClain, S. P., Batia, L. M., Pellegrino, M., Wilson, S. R., Kienzler, M. A., … Bautista, D. M. (2015). HTR7 Mediates Serotonergic Acute and Chronic Itch. *Neuron*, *87*(1), 124–138. http://doi.org/10.1016/j.neuron.2015.05.044

Myśliwiec, H., Baran, A., Harasim-Symbor, E., Choromańska, B., Myśliwiec, P., Milewska, A. J., … Flisiak, I. (2016). Increase in circulating sphingosine-1-phosphate and decrease in ceramide levels in psoriatic patients. *Archives of Dermatological Research*. http://doi.org/10.1007/s00403-016-1709-9

Olivera, A., Allende, M. L., & Proia, R. L. (2013). Shaping the landscape: Metabolic regulation of S1P gradients. *Biochimica et Biophysica Acta - Molecular and Cell Biology of Lipids*,

645 *1831*(1), 193–202. http://doi.org/10.1016/j.bbalip.2012.06.007

646 Patti, G., Yanes, O., Shriver, L., Courade, J.-P., Tautenhahn, R., Manchester, M., & Siuzdak, G.
647 (2008). Metabolomics implicates altered sphingolipids in chronic pain of neuropathic origin.
648 *Nature Chemical Biology*, *8*(3), 232–234. http://doi.org/10.1038/nchembio.767

649 Pinho-Ribeiro, F. A., Verri, W. A., & Chiu, I. M. (2017). Nociceptor Sensory Neuron–Immune
650 Interactions in Pain and Inflammation. *Trends in Immunology*, *38*(1), 5–19.
651 http://doi.org/10.1016/j.it.2016.10.001

652 Rivera, J., Proia, R. L., & Olivera, A. (2008). The alliance of sphingosine-1-phosphate and its
653 receptors in immunity. *Nature Reviews Immunology*, *8*(10), 753–763.
654 http://doi.org/10.1038/nri2400

655 Rogerio, A. P., Andrade, E. L., & Calixto, J. B. (2011). C-fibers, but not the transient potential
656 receptor vanilloid 1 (TRPV1), play a role in experimental allergic airway inflammation.
657 *European Journal of Pharmacology*, *662*(1–3), 55–62.
658 http://doi.org/10.1016/j.ejphar.2011.04.027

659 Roviezzo, F., Brancaleone, V., De Gruttola, L., Vellecco, V., Bucci, M., D'Agostino, B., … Cirino,
660 G. (2011). Sphingosine-1-phosphate modulates vascular permeability and cell recruitment
661 in acute inflammation in vivo. *The Journal of Pharmacology and Experimental*
662 *Therapeutics*, *337*(3), 830–837. http://doi.org/10.1124/jpet.111.179168

663 Roviezzo, F., Sorrentino, R., Bertolino, A., De Gruttola, L., Terlizzi, M., Pinto, A., … Cirino, G.
664 (2015). S1P-induced airway smooth muscle hyperresponsiveness and lung inflammation in
665 vivo: Molecular and cellular mechanisms. *British Journal of Pharmacology*, *172*(7), 1882–
666 1893. http://doi.org/10.1111/bph.13033

667 Sanna, M. G., Liao, J., Jo, E., Alfonso, C., Ahn, M. Y., Peterson, M. S., … Rosen, H. (2004).
668 Sphingosine 1-Phosphate (S1P) Receptor Subtypes S1P1 and S1P3, Respectively,
669 Regulate Lymphocyte Recirculation and Heart Rate. *Journal of Biological Chemistry*,
670 *279*(14), 13839–13848. http://doi.org/10.1074/jbc.M311743200

671 Sanna, Vincent, K. P., Repetto, E., Nhan, N., Brown, S. J., Abgaryan, L., … Gonzalez-Cabrera,
672 P. J. (2015). Bitopic S1P3 Antagonist Rescue from Complete Heart Block: Pharmacological
673 and Genetic Evidence for Direct S1P3 Regulation of Mouse Cardiac Conduction. *Molecular*
674 *Pharmacology*, *89*, 176–186. http://doi.org/10.1124/mol.115.100222

675 Schwab, S. R., Pereira, J. P., Matloubian, M., Xu, Y., Huang, Y., & Cyster, J. G. (2005).
676 Lymphocyte sequestration through S1P lyase inhibition and disruption of S1P gradients.
677 *Science (New York, N.Y.)*, *309*(5741), 1735–1739. http://doi.org/10.1126/science.1113640

678 Shimada, S. G., & LaMotte, R. H. (2008). Behavioral differentiation between itch and pain in
679 mouse. *Pain*, *139*(3), 681–687. http://doi.org/10.1016/j.pain.2008.08.002

680 Tominaga, M., Wada, M., & Masu, M. (2001). Potentiation of capsaicin receptor activity by
681 metabotropic ATP receptors as a possible mechanism for ATP-evoked pain and
682 hyperalgesia. *Proceedings of the National Academy of Sciences of the United States of*
683 *America*, *98*(12), 6951–6956. http://doi.org/10.1073/pnas.111025298

684 Trankner, D., Hahne, N., Sugino, K., Hoon, M. A., & Zuker, C. (2014). Population of sensory
685 neurons essential for asthmatic hyperreactivity of inflamed airways. *Proceedings of the*
686 *National Academy of Sciences*, *111*(31), 11515–11520.
687 http://doi.org/10.1073/pnas.1411032111

688 Tsunozaki, M., Lennertz, R. C., Vilceanu, D., Katta, S., Stucky, C. L., & Bautista, D. M. (2013). A
689 “toothache tree” alkylamide inhibits Aδ mechanonociceptors to alleviate mechanical pain.

The Journal of Physiology, *591*(Pt 13), 3325–40. http://doi.org/10.1113/jphysiol.2013.252106

Usoskin, D., Furlan, A., Islam, S., Abdo, H., Lönnerberg, P., Lou, D., … Ernfors, P. (2015). Unbiased classification of sensory neuron types by large-scale single-cell RNA sequencing Dmitry. *Nature Neuroscience*, *18*(1), 145–153. http://doi.org/10.1038/nn.3881

Wang, J., Kollarik, M., Ru, F., Sun, H., Mcneil, B., Dong, X., … Undem, B. (2017). Distinct and common expression of receptors for inflammatory mediators in vagal nodose versus jugular capsaicin-sensitive / TRPV1- positive neurons detected by low input RNA sequencing, 1–20.

Weth, D., Benetti, C., Rauch, C., Gstraunthaler, G., Schmidt, H., Geisslinger, G., … Kress, M. (2015). Activated platelets release sphingosine 1-phosphate and induce hypersensitivity to noxious heat stimuli in vivo. *Frontiers in Neuroscience*, *9*(April), 1–8. http://doi.org/10.3389/fnins.2015.00140

Wilson, S. R., Gerhold, K. a, Bifolck-Fisher, A., Liu, Q., Patel, K. N., Dong, X., & Bautista, D. M. (2011). TRPA1 is required for histamine-independent, Mas-related G protein-coupled receptor-mediated itch. *Nature Neuroscience*, *14*(5), 595–602. http://doi.org/10.1038/nn.2789

Wilson, S. R., Nelson, A. M., Batia, L., Morita, T., Estandian, D., Owens, D. M., … Bautista, D. M. (2013). The Ion Channel TRPA1 Is Required for Chronic Itch. *Journal of Neuroscience*, *33*(22), 9283–9294. http://doi.org/10.1523/JNEUROSCI.5318-12.2013

Yamashita-Sugahara, Y., Tokuzawa, Y., Nakachi, Y., Kanesaki-Yatsuka, Y., Matsumoto, M., Mizuno, Y., & Okazaki, Y. (2013). Fam57b (Family with sequence similarity 57, member B), a novel peroxisome proliferator-activated receptor y target gene that regulates

adipogenesis through ceramide synthesis. *Journal of Biological Chemistry*, *288*(7), 4522–4537. http://doi.org/10.1074/jbc.M112.440792

a

Gene Name
Ppargc1a
Fam57b
Esrrg
Esrrb
Lrp2
Spns1
Spns2
S1pr3
S1pr1

b

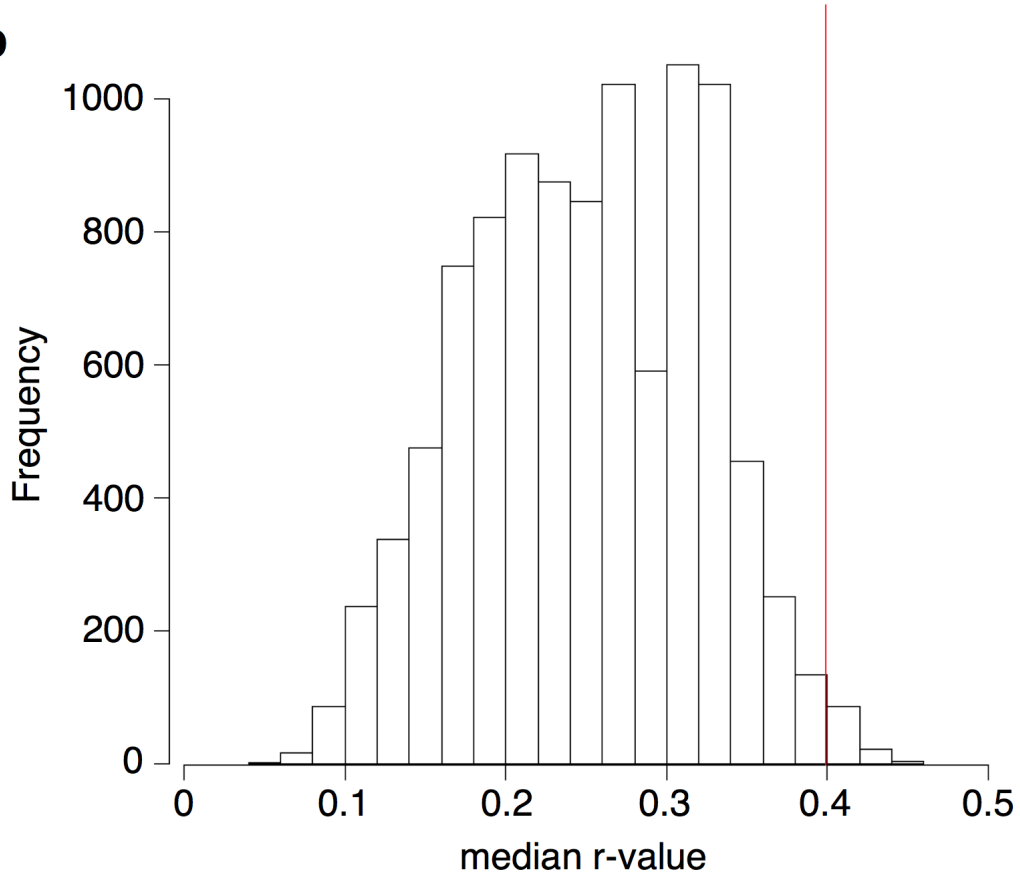

Figure 1

Figure 1. S1P pathway genes are positively correlated with chloroquine-evoked itch behaviors. a. Tabular list of the top 10 most highly expressed S1P pathway genes in DRG neurons. b. Histogram showing median absolute r-value for gene expression vs. itch plotted against frequency for 10,000 permutations of random subsets of 10 genes in the BXD DRG transcriptome. Red line indicates median r-value for S1P genes (r_{median} = 0.399, see Methods).

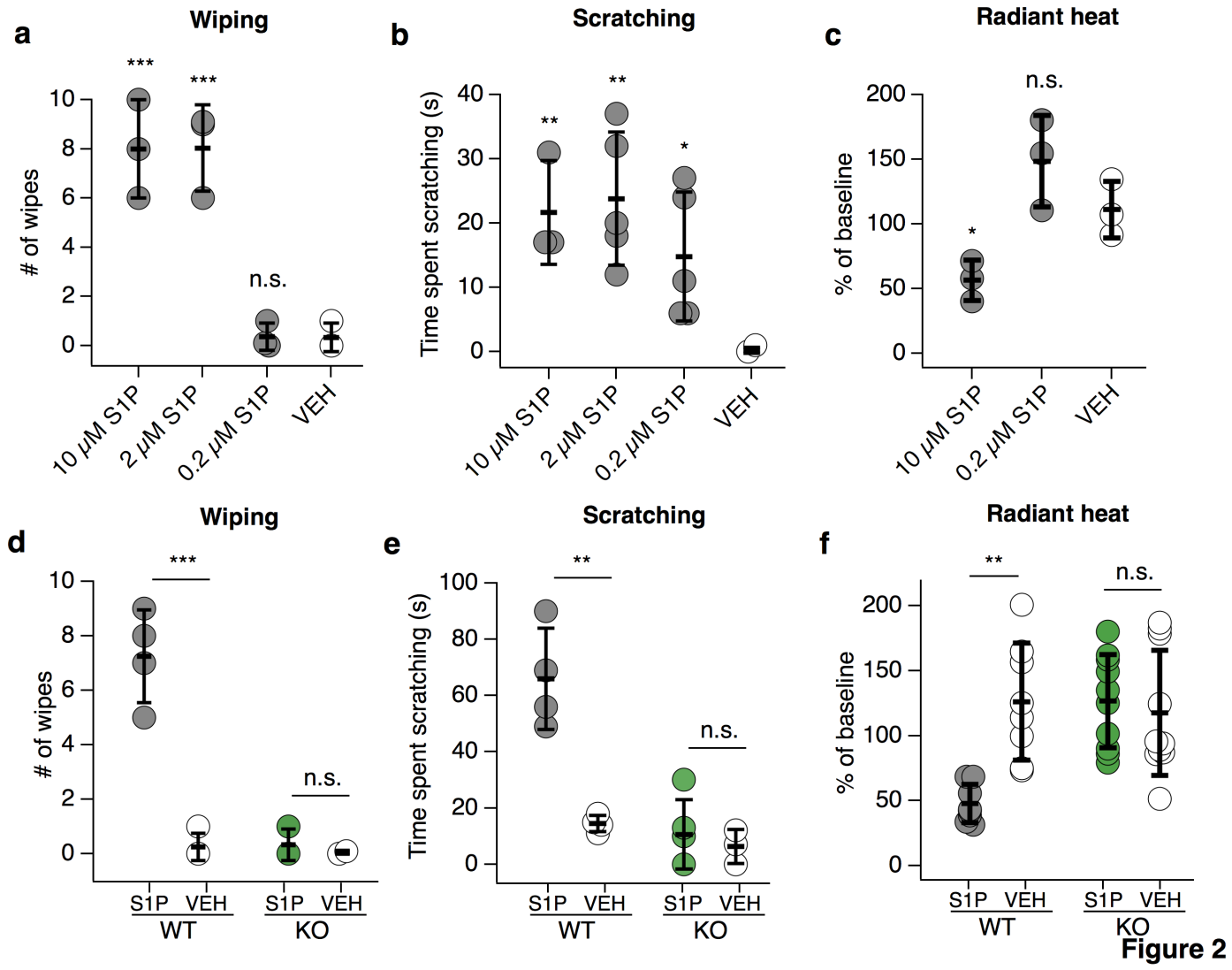

Figure 2. S1PR3 is the sole mediator of S1P-evoked pain and itch. a. Intradermal cheek injection of 10 μM S1P, 2 μM, 0.2 μM, and 20 μL 0.3% methanol PBS (vehicle), with quantification of number of forepaw wipes over the 5 minute post-injection interval; $p < 0.0001$ (one-way ANOVA ($F(3,8) = 30.67$); N = 3 mice per condition). Dunnett's multiple comparisons *p*-values are represented on graph for comparisons made between treated and vehicle groups. b. For same experiment in (a), quantification of time spent scratching over the 30-minute post-injection interval; $p = 0.0027$ (one-way ANOVA ($F(3,14) = 7.798$); N = 3-5 mice per condition). Dunnett's multiple comparisons *p*-values are represented on graph for comparisons made between treated and vehicle groups. c. Radiant heat normalized paw withdrawal latencies 20-30 minutes post injection of 15 μL 10 μM S1P, 0.2 μM S1P. or 0.3% methanol-PBS vehicle i.d. into the hind paw of wild-type mice; $p = 0.0129$ (one-way ANOVA ($F(2,6) = 9.8$); N = 3 mice per condition). Dunnett's multiple comparisons *p*-values are represented on graph for comparisons made between treated and vehicle groups. d. Number of wipes in response to intradermal injection of 20 μL 10 μM S1P or 0.3% methanol-PBS vehicle in cheek of age-matched *S1pr3* $^{+/-}$ and *S1pr3* $^{-/-}$ mice; $p < 0.0001$ (one-way ANOVA ($F(3,9) = 40.4$); N = 3-4 mice per condition). Dunnett's multiple comparisons *p*-values are represented on graph for comparisons made between treated and vehicle groups. e. Time spent scratching in response to intradermal injection of 20 μL 0.2 μM S1P or 0.1% methanol-PBS vehicle in rostral back of age-matched *S1pr3* $^{+/+}$ and *S1pr3* $^{-/-}$ mice; $p = 0.0089$ (one-way ANOVA ($F(3,9) = 7.274$); N = 3-4 mice per treatment). Dunnett's multiple comparisons *p*-values are represented on graph for comparisons made between treated and vehicle groups. f. Radiant heat normalized paw withdrawal latencies 20-30 minutes post injection of 15 μL 10 μM S1P or 0.3% methanol-PBS vehicle i.d. into the hind paw of age matched *S1pr3* $^{+/+}$ and *S1pr3* $^{-/-}$ mice; $p = 0.0004$ (one-way ANOVA ($F(3,32) = 7.964$); N = 8-10 mice per condition). Tukey's multiple comparisons *p*-values are represented on graph for comparisons made between treated and vehicle groups. Unless otherwise indicated, all error bars represent mean ± SD.

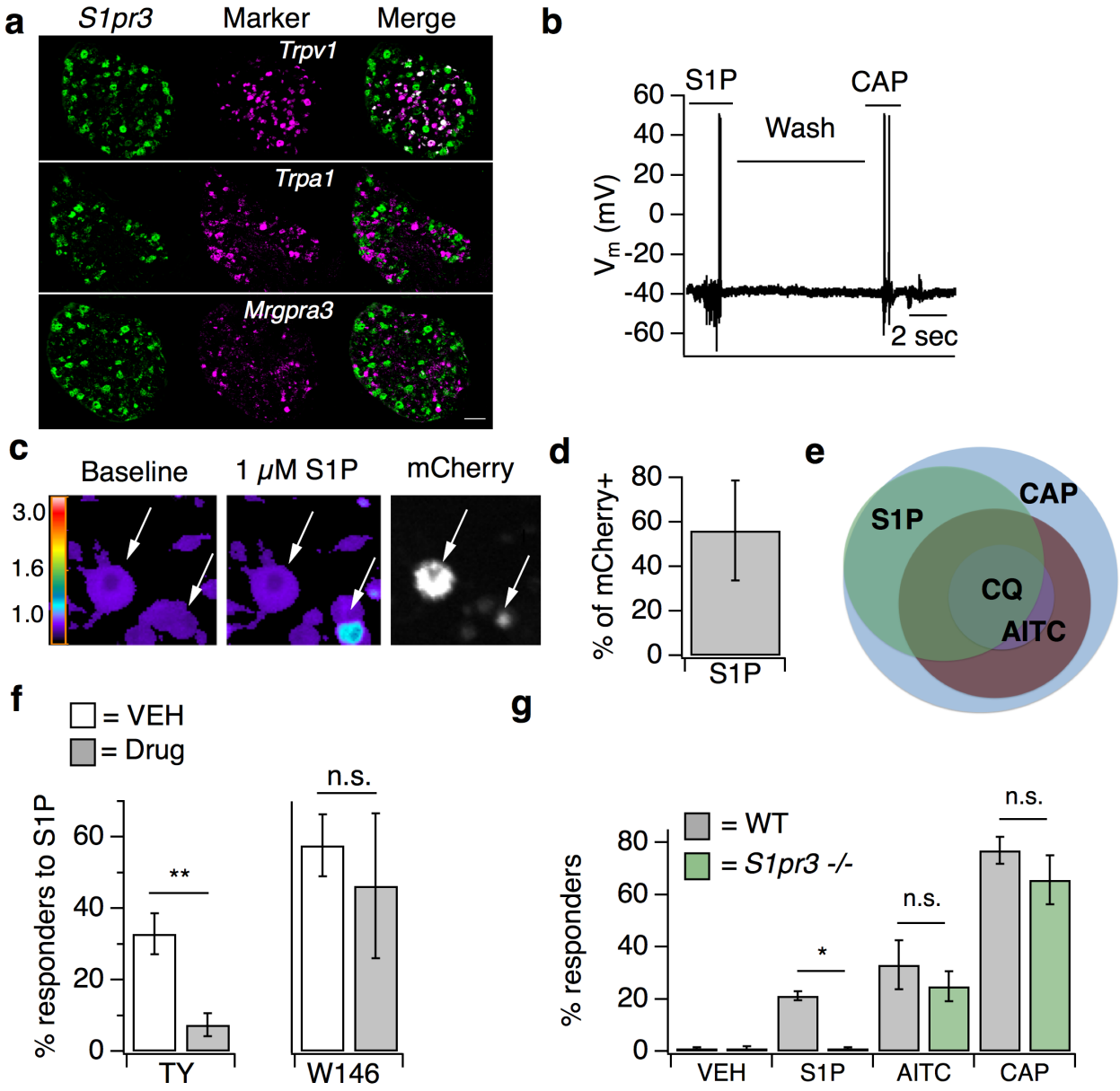

Figure 3

Figure 3. S1PR3 is expressed and functional in subsets of TRPV1+ thermal nociceptors and TRPA1+ pruriceptors. a. Co-ISH of *S1pr3* (green) with *Trpv1*, *Trpa1*, and *Mrgpra3* (magenta) in sectioned whole dorsal root ganglia from adult wild-type mice. Third column: overlay. Scale bar = 100 μm. Images were acquired using a 10x air objective. b. Current-clamp trace of a single neuron firing action potentials in response to bath addition of 1 μM S1P and 1 μM capsaicin. N = 4 of 10 neurons responded to S1P and N = 1 of 1 S1P-responsive also responded to capsaicin. c. (Top) Fura-2 AM calcium imaging before (left) and after (right) addition of 1 μM S1P in S1P3 $^{mCherry/+}$ cultured mouse DRG neurons. Bar indicates fluorescence ratio. Right-hand image indicates mCherry fluorescence. Arrows indicate an mCherry+/S1P- cell (right) and an mCherry+/S1P- cell (left). d. Percentage of mCherry+ DRG neurons which respond to 1 μM S1P (N = 274 neurons). Error bars represent mean response ± SD. e. Venn diagram demonstrating overlap of neuronal subpopulations activated by capsaicin, AITC, chloroquine, and S1P. Relative proportion of overlap represents % overlap as calculated from ratiometric calcium imaging data (N = 4,000 neurons). f. Effects of 100 μM TY 52156 (p = 0.0016 (two-tailed unpaired Student's t-test (t(6) = 5.42); N = 4 wells of 100 cells each)) or 1 μM W146 (p = 0.7921 (two-tailed unpaired Student's t-test (t(4) = 0.2817; N = 3 wells of 100 cells each)) on S1P responses of cultured DRG neurons. Error bars represent mean ± SD. g. Percent responders to S1P in age-matched wild-type and *S1pr3* $^{-/-}$ cultured DRG and TG neurons; $p < 0.0001$ (one-way ANOVA (F(7,95) = 4.764); N = 2 DRG and 2 TG preparations of 8 wells each). Sidak's multiple comparisons p-values are represented on graph for comparisons made between genotypes. Error bars represent mean ± SEM.

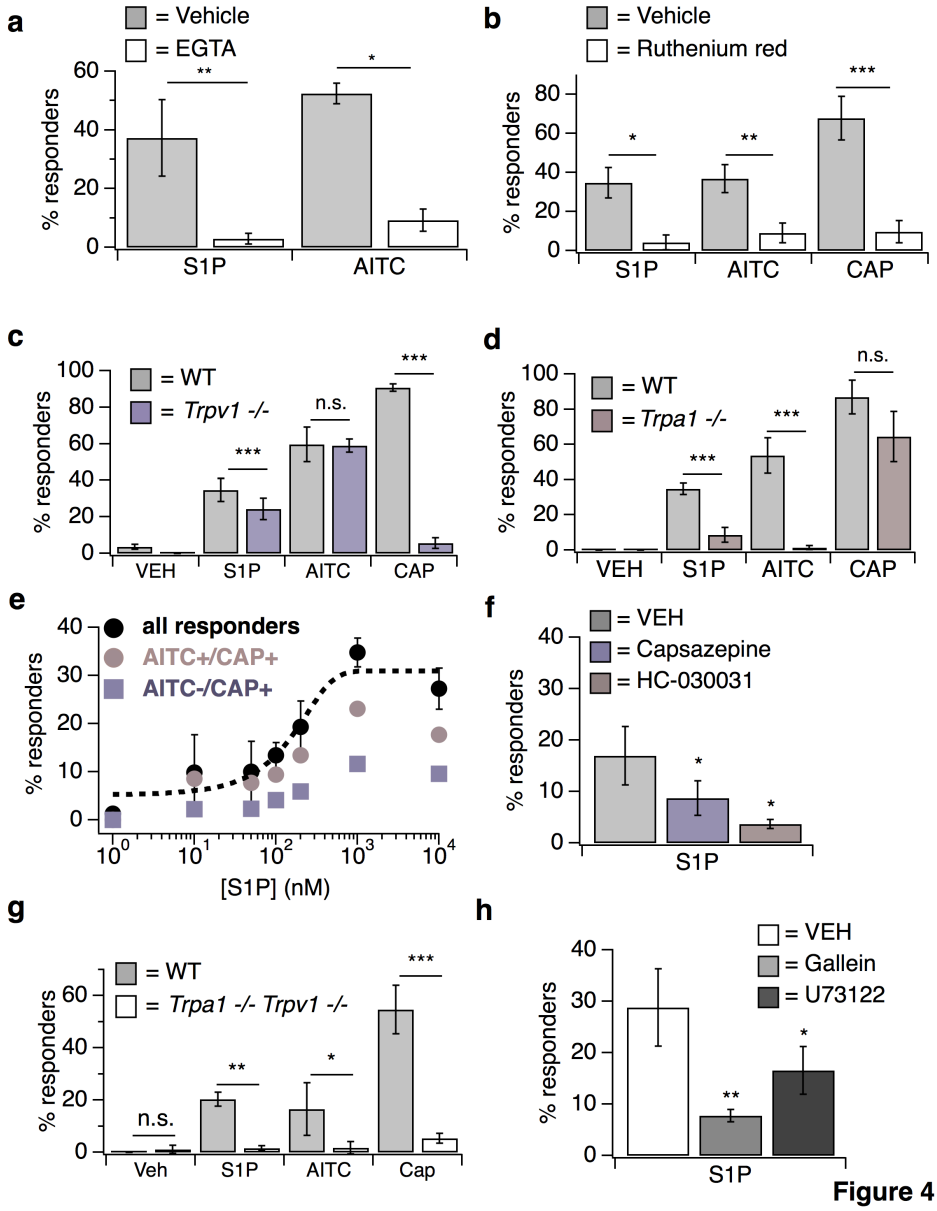

Figure 4

Figure 4. S1P activates sensory neurons via distinct TRPV1- and TRPA1-dependent mechanisms. a. Percent responders for vehicle, 1 μM S1P, AITC, and Cap in Calcium Ringer's- and 10 μM EGTA-Ringer's-treated DRG neurons; $p < 0.0001$ (one-way ANOVA ($F(3,11) = 8.291$); N = 4 wells of ~100 neurons each per treatment). Error bars represent mean ± SD. b. Percent responders for vehicle, 1 μM S1P, AITC, and Cap in vehicle treated and 10 μM Ruthenium Red-treated DRG neurons; $p < 0.0001$ (one-way ANOVA ($F(5,17) = 17.42$); N = 5 wells of ~100 neurons each per treatment). Error bars represent mean ± SD. c. Percent responses for 1 μM S1P in +/+ and *Trpv1* -/- neurons; $p < 0.0001$ (one-way ANOVA ($F(7, 179) = 72.67$); N = 3 age-matched mice per genotype). Error bars represent mean responses ± SEM. d. Percent responses for 1 μM S1P in +/+ and *Trpa1* -/- neurons; $p < 0.0001$ (one-way ANOVA ($F(7,210) = 105$); N = 3 age-matched mice per genotype). Error bars represent mean responses ± SEM. e. Dose-response curve of mean neuronal responses to varying concentrations of S1P. Concentrations used: 1, 10, 50, 100, 200, 1000, and 10,000 nanomolar. Error bars represent mean ± SD (N = 2 animals). Black dotted line indicates sigmoidal fit for all S1P responders from which EC_{50} was derived. Colored traces indicate proportion of neurons responding to S1P and AITC or S1P and capsaicin at indicated concentrations. f. Effect of 50 μM Capsazepine (TRPV1 antagonist) and 50 μM HC-030031 (TRPA1 antagonist) vs. DMSO-Ringer's vehicle on S1P-evoked calcium responses in cultured DRG neurons; $p < 0.0001$ (one-way ANOVA ($F(8,30) = 84.32$); N = 3 wells of ~100 neurons each per treatment) Error bars represent mean responses ± SD. g. Percent responses for vehicle, 1 μM S1P, AITC, and Cap in *Trpa1/Trpv1* $^{+/+}$ and $^{-/-}$ DRG neurons; $p < 0.0001$ (one-way ANOVA ($F(7,40) = 8.555$); N = 2 age-matched mice per genotype) Error bars represent mean ± SD. h. Percent S1P responders as a fraction of total neurons pre-incubated 15 minutes with either DMSO-Ringer's vehicle, 1 μM U73122 (PLC blocker), or 100 μM Gallein (Gβγ blocker); $p = 0.0030$ (one-way ANOVA ($F(3,8) = 11.32$); N = 3 wells of ~100 neurons each per treatment). Error bars represent mean responses ± SD. Unless otherwise indicated, Sidak's multiple comparisons were made between treated and vehicle for each agonist.

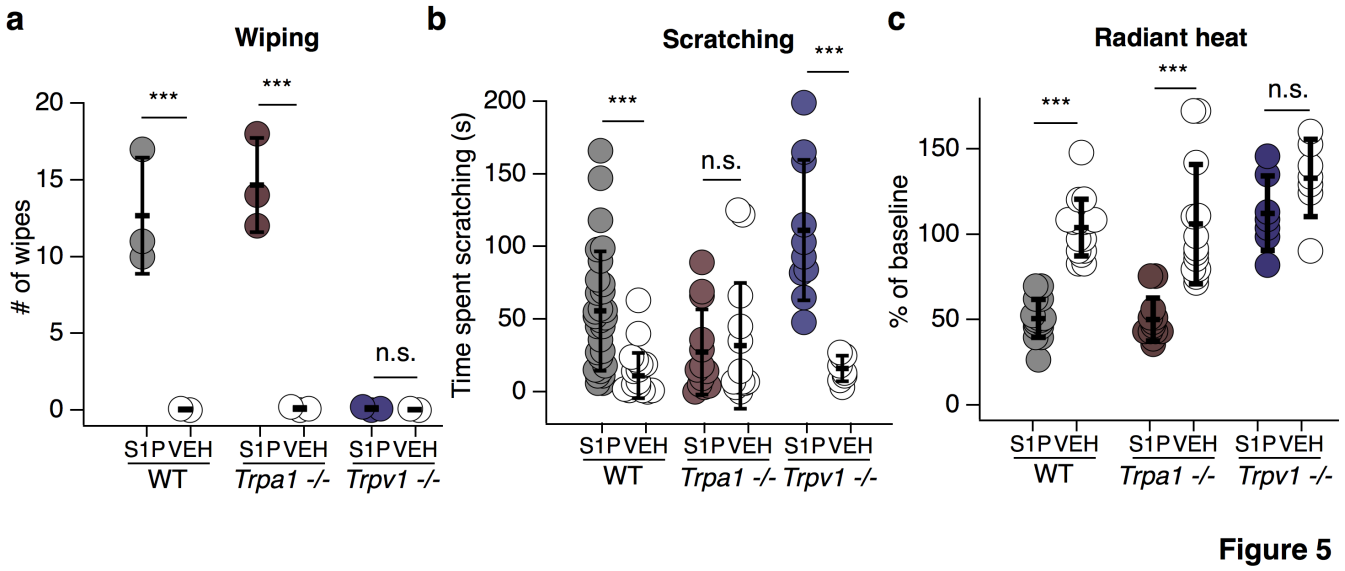

Figure 5. S1P elicits pain and itch via distinct molecular pathways. a. Number of wipes in response to intradermal injection of 20 µL 10 µM S1P or 0.3% methanol-PBS vehicle in cheek of age-matched wild-type, *Trpa1* $^{-/-}$ and *Trpv1* $^{-/-}$ mice; $p < 0.0001$ (one-way ANOVA ($F(5,11) = 33.98$); N = 3 age-matched mice per condition). Error bars represent mean ± SD. b. Time spent scratching in response to intradermal injection of 20 µL 0.2 µM S1P or 0.1% methanol-PBS vehicle in rostral back of age-matched wild-type, *Trpa1* $^{-/-}$ and *Trpv1* $^{-/-}$ mice; $p < 0.0001$ (one-way ANOVA ($F(5,91) = 14.13$); N = 8 or more age-matched mice per condition). Error bars represent mean ± SD. c. Radiant heat normalized paw withdrawal latencies 20-30 minutes post injection of 15 µL 10 µM S1P or 0.3% methanol-PBS vehicle i.d. into the hind paw of age matched wild-type, *Trpa1* $^{-/-}$ and *Trpv1* $^{-/-}$ mice; $p < 0.0001$ (one-way ANOVA ($F(5,66) = 31.23$); N = 7 or more age-matched mice per condition). Error bars represent mean ± SD. For all graphs, Sidak's multiple comparisons were made between treated and vehicle for each genotype.

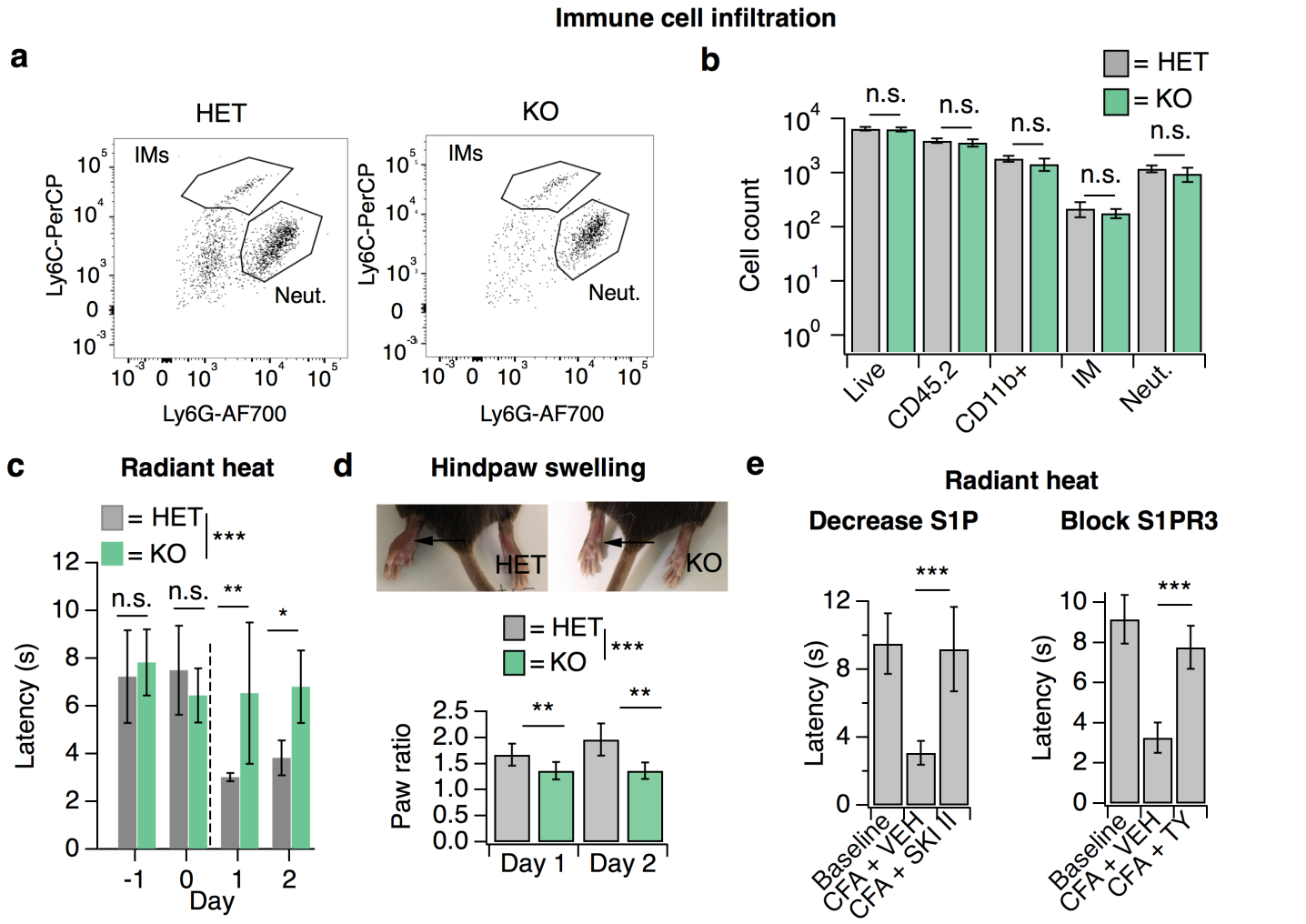

Figure 6

Figure 6. S1P and S1PR3 are essential for chronic thermal hypersensitivity. a. Recruitment of neutrophils (Neut.) or inflammatory monocytes (IMs) to hindpaw skin 24 hours post-CFA administration in HET and KO mice, as a dot plot of CD11b+ cells plotting Ly6G fluorescence intensity vs. Ly6C intensity (AFU). Boxes are for illustrative purposes. b. Recruitment of immune cells, including neutrophils (Neut.) and inflammatory monocytes (IMs) to hindpaw skin 24 hours post-CFA administration in HET (grey) and KO (green) mice, displayed as total number of cells; N = 8 mice per genotype. Sidak's multiple comparisons were made between HET and KO for each cell type. c. Thermal latency before and after CFA treatment (indicated by dotted line); $p_{genotype}$ = 0.0053 (two-way ANOVA (F(1,8) = 14.36); N = 5 mice per genotype). Sidak's multiple comparison between genotypes for specific time points indicated on graph. Error bars represent mean ± SD. d. (Top) Images of HET and KO littermate mice 48 hours after CFA injection into the left paw (arrows). (Bottom) Hindpaw swelling of CFA-treated paw compared to PBS-treated paw as measured to the nearest 1/10th mm 24- and 48-hours post CFA injection; ; $p_{genotype}$ = 0.0003 (two-way ANOVA (F(1,8) = 9.64); N = 5 mice per genotype). Error bars represent mean ± SD. e. (Left) Thermal latency assessed before and after CFA injection (arrow) with either vehicle (VEH) or SKI II acutely administered on Day 1; $p < 0.0001$ (one-way ANOVA (F(2,21= 19.16); N = 5-7 mice per treatment). Dunnett's test comparisons to baseline are indicated on graph. (Right) Thermal latency assessed before ("Baseline") and 24 hours post CFA injection with either vehicle (CFA + VEH) or TY 52156 (CFA + TY) acutely administered; $p < 0.0001$ (one-way ANOVA (F(2,17= 50.44); N = 5 mice per treatment). Dunnett's test comparisons to baseline are indicated on graph. Error bars represent mean ± SD.

a

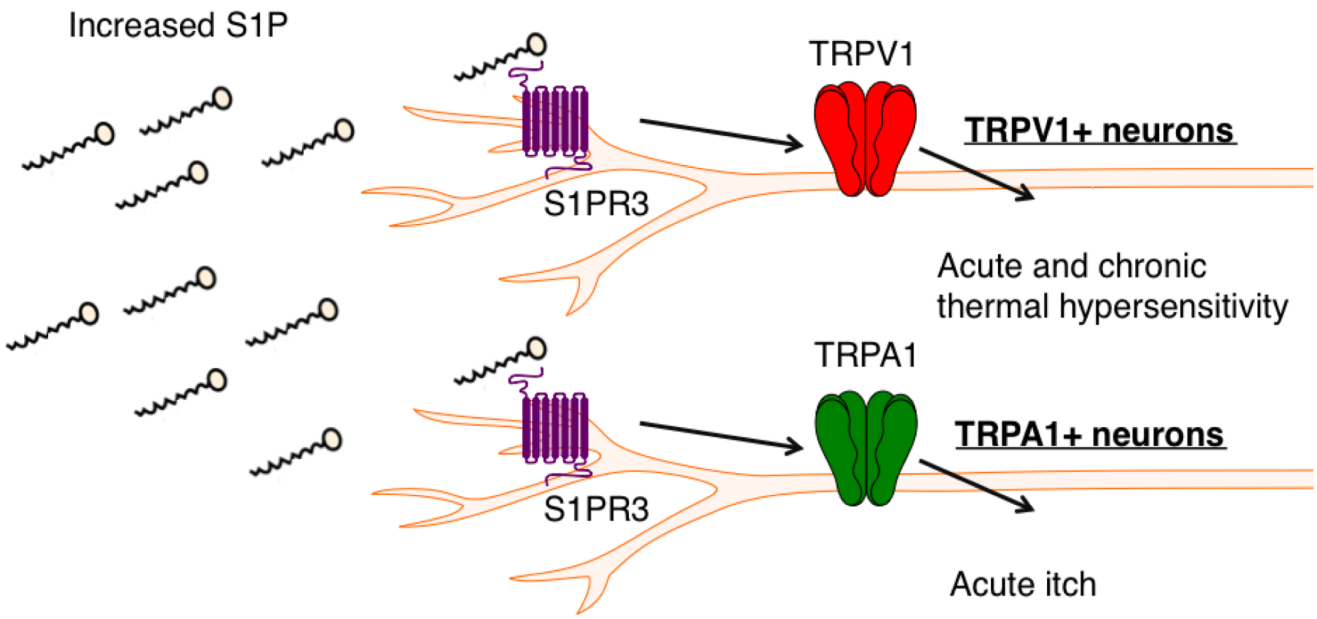

Figure 7

Figure 7. Model of the effects of elevated S1P on S1PR3-dependent thermal hypersensitivity and acute itch in sensory neurons. a. Elevated S1P can 1) elicit thermal hypersensitivity or acute pain via S1PR3-dependent activation of TRPV1 (top) and 2) elicit itch-evoked scratching via S1PR3-dependent activation of TRPA1.